On the Response of the Ocean to a Moving Storm: The Nonlinear Dynamics

RICHARD J. GREATBATCH

Department of Applied Mathematics and Theoretical Physics, University of Cambridge, Cambridge, CB3 9EW, England

(Manuscript received 1 April 1982, in final form 28 October 1982)

ABSTRACT

A novel and efficient numerical method is used to investigate the nonlinear equations of motion for the upper layer of a two-layer ocean in which the lower layer is infinitely deep and at rest. The efficiency is achieved by seeking solutions that are in a steady state, translating in equilibrium with the storm. Oscillations are found in the wake of the storm. Two features of the response are attributed to the nonlinear terms in the equation of motion: 1) a rapid transition from a maximum in the downwelling phase, to a maximum in the upwelling phase of each oscillation, followed by a gradual relaxation to the next downwelling maximum; and 2) a displacement of the maximum response, usually to the right of the storm track, by ~40 km. It is shown that the horizontal pressure gradient terms can be neglected from the momentum equations for "fast", "large" storms, in which case a Lagrangian integration can be performed, following fluid particles. This enables feature 1) to be attributed to the along-track advection terms and 2) to be associated with the cross-track advection terms. When the horizontal pressure gradient terms are more important, feature 1) remains, but the maximum response is displaced, in the wake, to the left of the track from the right. It is shown that even a symmetric storm can produce a strongly asymmetric response. Finally, results are compared with observations of the response of the ocean to hurricanes.

1. Introduction

In this paper we consider the response of the ocean to a single, isolated, moving storm. The situation to which this is most applicable in nature is that of a moving hurricane, but the same ideas would apply to an extratropical storm. Hurricanes are particularly strong forcing events for the ocean, and we would anticipate nonlinearity to play an important role in the dynamics. We take as our basic model a two-layer baroclinic ocean in which the lower layer is infinitely deep and at rest. The details of the model are described in Section 2. In Section 3, the frictionless equations of motion, with the wind forcing modeled as a body force, are integrated using a novel and efficient numerical procedure in which we seek solutions that are in a steady state, translating in equilibrium with the storm. The results compare well with those of Chang and Anthes (1978) if allowance is made for the decrease in amplitude associated with the inclusion of mixed-layer effects in their model.

In Section 4, a scale analysis is carried out suggesting that, on the time scale of a few inertial periods, the dominant balance in the equations of motion is often between the Coriolis and inertia terms, in which case the horizontal pressure gradient terms in the momentum equations can be neglected as a first approximation. A Lagrangian integration can then be performed, following individual fluid particles, and this is done in Section 5. Good agreement with the numerical solutions obtained in Section 3 is obtained, demonstrating the validity of the procedure. Furthermore, the reasons for the along-track and cross-track nonlinear effects can be identified and quantified.

In Section 6, consideration is given to changes that occur when the horizontal pressure gradient terms are more important in the momentum equations, and in Section 7, the effect of asymmetry in the storm forcing is investigated. Finally, in Section 8 we summarize the results and their relation to observed features of hurricane response.

2. The model equations

We consider the solution where, relative to a frame of reference moving with speed U in the x-direction, both the storm and the response to it are in a steady state. The velocity (u, v) in the upper layer and the depth h of the layer are then functions only of the two variables $\xi = Ut - x$ and the cross-track coordinate y. The upper layer has density ρ_1 and lies over an infinitely deep, resting, lower layer of density ρ_2. The equations are

$$(U - u)u_\xi + vu_y - fv = p_\xi + X, \quad (2.1a)$$

$$(U - u)v_\xi + vv_y + fu = -p_y + Y, \quad (2.1b)$$

$$(U - u)p_\xi + vp_y + p(-u_\xi + v_y) = 0, \quad (2.1c)$$

where f is the Coriolis parameter (assumed constant), $p = g'h$ where $g' = g(\rho_2 - \rho_1)/\rho_1$ is the reduced gravity,

and (X, Y) represents the forcing taken to be given by

$$(X, Y) = \left(\frac{\tau_x}{\rho_1 H}, \frac{\tau_y}{\rho_1 H}\right), \tag{2.2}$$

where $\tau = (\tau_x, \tau_y)$ is the surface wind stress. The depth H is taken as the undisturbed layer depth and is fixed throughout the integration. In this way, (2.2) can provide a realistic wind forcing field, even though turbulent entrainment has been neglected. It is convenient to follow Chang and Anthes (1978), and model the wind stress τ as

$$(\tau_r, \tau_\theta) = (-\tau_{r_{\max}}, \tau_{\theta_{\max}}) \times \begin{cases} r/r_{\min} & (0 \leq r \leq r_{\min}) \\ (r_{\max} - r)/(r_{\max} - r_{\min}) & (r_{\min} \leq r \leq r_{\max}) \\ 0 & (r_{\max} \leq r), \end{cases} \tag{2.3}$$

where τ_r and τ_θ are the radial and tangential components of the stress with respect to the storm center, and r is the radial distance from the center. We put $r_{\min} = 30$ km, $r_{\max} = 300$ km, $\tau_{r_{\max}} = 1$ N m^{-2} and $\tau_{\theta_{\max}} = 3$ N m^{-2}, suitable for hurricane forcing. An asymmetric storm will be considered in Section 7.

It is also convenient to begin by choosing the model parameters to coincide with those of Chang and Anthes (1978) who also worked with the same basic model of a two-layer baroclinic ocean. We therefore put $H = 50$ m, $c = (g'H)^{1/2} = 1$ m s^{-1} (corresponding to a temperature difference between the two layers of 10°C) and $f = 7.5 \times 10^{-5}$ s^{-1}. The Rossby radius of deformation is then 13.3 km.

Geisler (1970) showed that for a linear model, when the storm translation speed U is greater than the wave speed c, the equations are hyperbolic in character and the ocean is undisturbed ahead of the storm. This is because the group velocity for inertia–gravity waves is bounded above by c. The same will be expected to hold for the nonlinear equations. This is the only case we shall consider and we shall, therefore, assume that

$$u = v = 0 \quad \text{and} \quad p = c^2 \text{ ahead of the storm.} \tag{2.4}$$

In practice, (2.4) will be applied at the leading edge of the storm, $\xi = \xi_0$, say, the wind stress being zero throughout the region $\xi \leq \xi_0$.

3. The numerical method and calculated solutions

It was remarked at the end of the previous section that when $U > c$, the ocean is undisturbed ahead of the storm. With this as our initial condition, applied at $\xi = \xi_0$, the problem becomes an initial value problem in the time variable ξ. This is the approach adopted here to integrate (2.1). The method can be thought of as either integrating to find the time development of the solution along a line of points perpendicular to the storm track, or integrating backward from a line of points perpendicular to the storm track ahead of the storm to find the spatial distribution of the solution at a given time. The variables u and p are stored at the same points along this line, with v at intermediate points, corresponding to the Arakawa C-grid (Arakawa and Lamb, 1977). The leap-frog scheme is used in time (ξ), with second-order, centered differencing in space (y). The finite difference form of (2.1a) and (2.1c) yields, at each time step, two simultaneous equations for the new values of u and p, u^{n+1} and p^{n+1}, i.e.,

$$u^{n+1}(U - u^{n+1/2}) - p^{n+1} = F^{n+1/2},$$
$$p^{n+1}(U - u^{n+1/2}) - p^{n+1/2}u^{n+1} = G^{n+1/2},$$

where n is the time index and $F^{n+1/2}$ and $G^{n+1/2}$ are known quantities. These are easily solved to obtain u^{n+1} and p^{n+1}. The detailed properties of the numerical method are discussed elsewhere (Greatbatch, 1982a). It is sometimes desirable to apply some Laplacian smoothing in space (y) to control nonlinear instability, and a very mild time smoothing in time (ξ) to control time splitting. The grid spacing, perpendicular to the storm track, is fixed at 20.7 km; that along the track at 15.5 km. The solutions remain basically unchanged when the resolution is tripled. Free-slip boundary conditions are applied at the edges of the cross-track grid (It can be shown that no significant reflection occurs on the time scale considered here.)

Fig. 1 shows the computed horizontal divergence

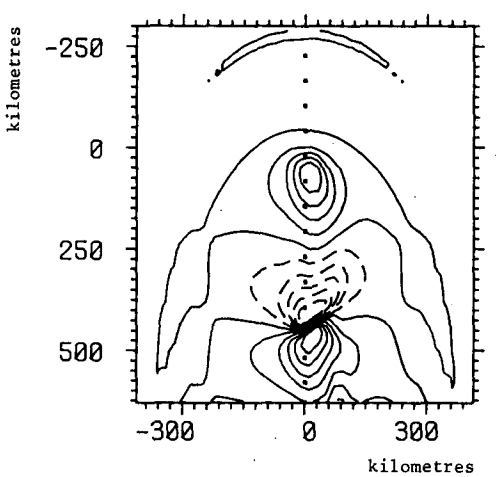

FIG. 1. The horizontal divergence field expressed as the equivalent vertical velocity at the undisturbed layer depth H for a storm translating at 5 m s^{-1}. In this case $H = 50$ m and the reduced gravity g' is such that the wave speed $(g'H)^{1/2}$ is 1 m s^{-1}. The contour interval is 5.1×10^{-4} m s^{-1} and is one-sixth of the maximum response. The dashed contours denote downwelling. The zero contour and contours denoting upwelling are shown as solid lines. The coordinates are measured from the storm center, the along-track coordinate increasing behind the storm. The track of the storm center is shown by the dotted line.

field, expressed as the equivalent vertical velocity at 50 m depth, for a storm translating at 5 m s^{-1}. The center of the storm is located at the origin of the coordinate axes. The storm is translating up the center of the figure, the storm track being indicated by the dotted lines. Fig. 2 shows the equivalent picture from Chang and Anthes (1978). It is important to realize that in their model, both horizontal space dimensions are retained, the storm being "initiated" at the beginning of the integration and then moved across the grid. Their model also included turbulent entrainment, which accounts for the difference in amplitude between the two solutions. The horizontal scales are the same in both figures. It is apparent that the new model reproduces all the essential features found in Chang and Anthes' model, with the considerable saving in computer resources obtained by eliminating the along-track coordinate. Turbulent entrainment has been included in an extended version of the model which also includes a realistic vertical structure (Greatbatch, 1982b).

The along-track wavelength can be estimated by extending the integration further behind the storm and is found to be near 420 km. The local inertial wavelength ($2\pi U/f$) is also 420 km. Two important features of the oscillation are as follows:

1) The upwelling and downwelling phases are not evenly distributed throughout the oscillation, there being a rapid transition from a maximum in the downwelling phase to a maximum in the upwelling phase, followed by a gradual transition to the next downwelling maximum.

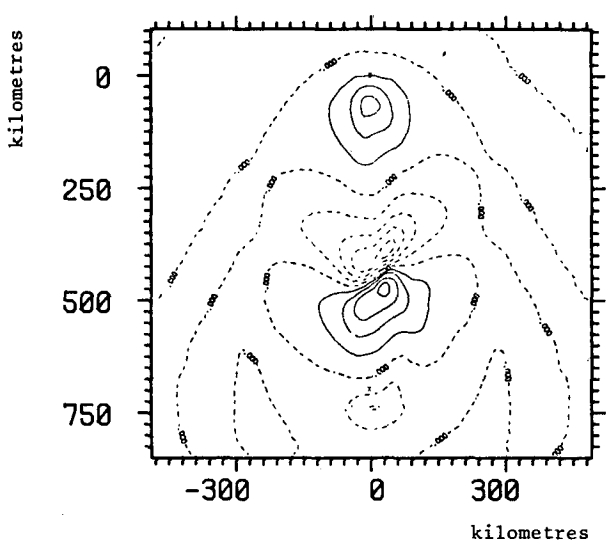

FIG. 2. The vertical velocity field obtained by Chang and Anthes (1978) for a storm translating at 5 m s^{-1} and an undisturbed layer depth H of 50 m and wave speed $(g'H)^{1/2}$ of 1 m s^{-1}. The coordinates and scale are as in Fig. 1. The contour interval is 2.5 $\times 10^{-4}$ m s^{-1}, the solid contours denoting downwelling, the dashed upwelling.

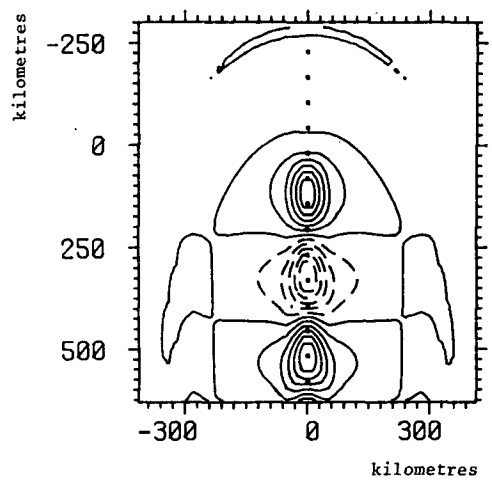

FIG. 3. The equivalent of Fig. 1, obtained by integrating the equations obtained by linearizing about the undisturbed state. The contour interval is 5.0 $\times 10^{-4}$ m s^{-1} and is one-sixth of the maximum response.

2) The maximum response occurs ~40 km to the right of the storm track (when viewing the storm from behind).

Both these features are a direct consequence of the nonlinearity in the equations of motion, as can be seen by comparison with Fig. 3, which is the equivalent picture to Fig. 1, obtained by integrating the equations of motion linearized about the initial, undisturbed state. The symmetry of the linear solution about the storm track is a consequence of the radial symmetry of the forcing field (2.3).

The results (not shown) obtained by integrating with storms translating at 10 and 2.5 m s^{-1} also compare very favorably with those obtained by Chang and Anthes, with the two features 1) and 2) referred to above occurring in both cases, although in the 10 m s^{-1} case these features are less pronounced, indicating that the nonlinear terms in the equations of motion are playing a less important role. This is discussed later in Section 5. The along-track wavelengths were estimated to be near 835 and 195 km, respectively, in these two cases, compared with the corresponding local inertial wavelengths of 838 and 209 km.

A useful check on the numerical method is provided by the conservation of potential vorticity in the wake of the storm. In fact

$$\frac{D}{Dt}\left(\frac{\zeta + f}{p}\right) = (-Y_\xi - X_y)/p, \qquad (3.1)$$

where here, $\zeta = -v_\xi - u_y$ is the relative vorticity and

$$\frac{D}{Dt} \equiv (U - u)\frac{\partial}{\partial \xi} + v\frac{\partial}{\partial y}$$

is the total derivative following fluid particles. Con-

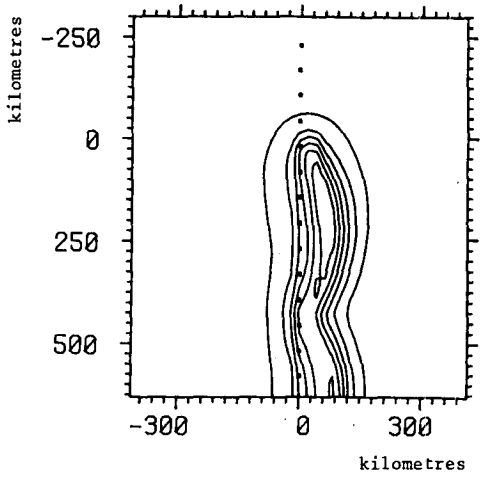

FIG. 4. The potential vorticity field corresponding to the horizontal diveregence field shown in Fig. 1. The contour interval is 3.1×10^{-7} m^{-1} s^{-1} and is one-sixth of the maximum attained value. In the wake of the storm, the contours should coincide with the particle paths. The coordinates and scale are as in Fig. 1.

tours of the potential vorticity $[(\zeta + f)/p]$ are shown in Fig. 4. It can be seen that the model does, indeed, conserve potential vorticity in the wake of the storm. In this region, the contours should coincide with the particle paths (these are discussed in detail in Section 5, where they are obtained by a different method).

4. Scale analysis

In this section, we use scale analysis to investigate the dominant balances in the equations of motion (2.1). To do this we let V be a characteristic velocity scale for the response (that the components u, v have the same scale V is apparent from the velocity field obtained from the integrations described in the previous section, although not presented here) and L a length scale characteristic of the width of the response across the storm track.[1] We take U/f as our length scale along the storm track in accordance with the observation in the previous section that the dominant wavelength along the track is close to the local inertial wavelength $2\pi U/f$. Some variation in the length scale of the response along the track was also noted [feature 1) described in the previous section]. It turns out, however, that the regions over which this length scale is comparatively small (where, in fact, the following scale analysis would break down) are not important in determining the structure of the response over the time scales to be considered here, as will be seen in Section 5.

We shall take $1/f$ as our time scale following fluid particles [i.e., $D/Dt = O(f)$] and c^2 as our characteristic value for p. It then follows from (2.1c) that the change in p, i.e., Δp, has order

$$\Delta p = O(c^2V/U, c^2V/Lf), \tag{4.1}$$

the first term in (4.1) corresponding to the u_ξ term and the second term to the v_y term in the horizontal divergence. It then follows that

$$p_\xi = O(c^2Vf/U^2, c^2V/UL), \tag{4.2a}$$

$$p_y = O(c^2V/UL, c^2V/L^2f). \tag{4.2b}$$

It then follows immediately that the horizontal pressure gradient terms will be small compared to the Coriolis terms in (2.1a) and (2.1b) if

$$c^2/U^2 \ll 1, \tag{4.3a}$$

$$c^2/f^2L^2 \ll 1. \tag{4.3b}$$

Eq. (4.3a) is the condition that the square of the ratio of the non-rotating wave speed c to the translation speed U is small compared to 1, and (4.3b) is the condition that the square of the ratio of the Rossby radius of deformation c/f to the width scale of the response across the storm track be small compared to 1. Combining these, we can say that the conditions (4.3a) and (4.3b) correspond to having "fast-moving" and "large" storms, respectively.

We conclude that on a time scale of a few inertial periods, if (4.3a) and (4.3b) are both satisfied, then we would expect the horizontal pressure gradient terms in (2.1a) and (2.1b) to be small compared with the Coriolis terms so that the dominant balance is between the inertia terms and the Coriolis terms. It is important to realize that the horizontal pressure gradient terms are crucial to the dispersion of energy away from the storm track in the geostrophic adjustment process and cannot be neglected on time scales characteristic of that process.

In the experiments described in the previous section, we took $c = 1$ m s^{-1} so that $c/U = 0.2$, 0.1 and 0.4 for storms translating at 5 m s^{-1}, 10 m s^{-1} and 2.5 m s^{-1}, respectively. This gives $(c/U)^2 = 0.04$, 0.01 and 0.16, so that we could reasonably expect (4.3a) to be satisfied for the storms translating at 5 and 10 m s^{-1} with more significant second-order effects in the case of the storm translating at 2.5 m s^{-1}.

To estimate the ratio c/fL we need to assign values to L. We can do this by estimating the scale L from the numerical results described in the previous section. A value of 100 km was assigned for each of the three translation speeds considered. For the Rossby radius used here of 13.3 km, this gives $c/fL = 0.13$. $(c/fL)^2$ then has the value 0.02 so that we would expect (4.3b) to be satisfied in each case.

We conclude that we would expect the dominant balance in the equations of motion to be between the inertia terms and the Coriolis terms on the time scale

[1] L is also the scale of the forcing, see Greatbatch (1982a).

of a few inertial periods in the cases considered here, with this approximation being less good in the case of the storm translating at 2.5 m s^{-1}. In fact, in the 2.5 m s^{-1} case, it is the p_ξ term that is likely to be more important, as can be seen by substituting the appropriate values for the scales in (4.2). This accounts for the shortening of the wavelength along the track compared with the inertial wavelength in this case, noted in the last section. To understand this, we note that the dispersion relation obtained from linear theory is

$$\omega^2 = (f^2 + c^2k^2)/(U^2 - c^2),$$

where ω is the along-track wavenumber and k is the cross-track wavenumber. In this case $(ck)^2 \ll f^2$ [this is (4.3b)] so

$$\omega^2 \approx f^2/(U^2 - c^2).$$

The along-track wavelength is, therefore, shortened compared to the inertial wavelength, by the factor $(U^2 - c^2)^{1/2}/U = 0.92$ in this case. This gives an along track wavelength of 192 km., compared with 195 km, estimated from the model results.

5. A simple Lagrangian model

In this section, we exploit the conclusion of the last section and drop the horizontal pressure gradient terms p_ξ and p_y from (2.1a) and (2.1b). We can then write (2.1a) and (2.1b) in Lagrangian form as

$$\frac{du}{dt} - fv = X[x(t), y(t), t], \tag{5.1a}$$

$$\frac{dv}{dt} + fu = Y[x(t), y(t), t], \tag{5.1b}$$

where d/dt is the rate of change in time for a particular fluid particle. $[x(t), y(t)]$ is the position of that particle at time t, and $[u(t), v(t)]$ is the velocity of the particle at time t. In fact

$$\frac{dx}{dt} = u(t), \tag{5.1c}$$

$$\frac{dy}{dt} = v(t). \tag{5.1d}$$

The problem is now reduced to solving the system of ordinary differential equations (5.1) for the variables $u(t)$, $v(t)$, $x(t)$, $y(t)$. We do this, numerically, for a grid of points perpendicular to the storm track, initially ahead of the storm, for each of the three cases of storms translating at 5, 10 and 2.5 m s^{-1}. The output from the model consists of an irregular grid of points given by the positions $[x(t), y(t)]$ of each particle after each time step, with u and v specified at each of these points. The horizontal divergence field $\delta = u_x + v_y$ and the relative vorticity field $\zeta = v_x - u_y$ can then be estimated at each point (see the Appendix for a detailed discussion of the method used). The depth of the upper layer h is then found using (2.1c) written in the form

$$\frac{dp}{dt} + p\delta = 0,$$

where, once again, $p = g'h$. This enables us to calculate the potential vorticity $(\zeta + f)/p$, which again provides a useful check on the numerical method [Eq. (3.1) still holds in the reduced system].

Fig. 5 shows the horizontal divergence field obtained for a storm translating at 5 m s^{-1} and is equivalent to Fig. 1, which shows the horizontal divergence field obtained by integrating the full equations (2.1). It is clear that the reduced, Lagrangian model is capable of reproducing both the amplitude and structure of the solution, demonstrating that on this time scale, in the cases considered, the horizontal pressure gradient terms do not play an important role in the governing equations. In particular, the two main features 1) and 2) of the response shown in Fig. 1, and discussed in Section 3, are reproduced. A similar striking agreement is obtained for storms translating at 10 and 2.5 m s^{-1} (see Table 1) except for the discrepancy in the along-track wavelength noted for the 2.5 m s^{-1} case in the last section. The conservation of potential vorticity along particle paths in the wake of the storms has been verified in each case.

The key to understanding the role of the nonlinear terms in the equations of motion in shaping the response is found by examining the individual particle paths collectively. Fig. 6 shows the computed particle paths for a storm translating at 5 m s^{-1}. This can be compared with Fig. 4 in which the contours in the

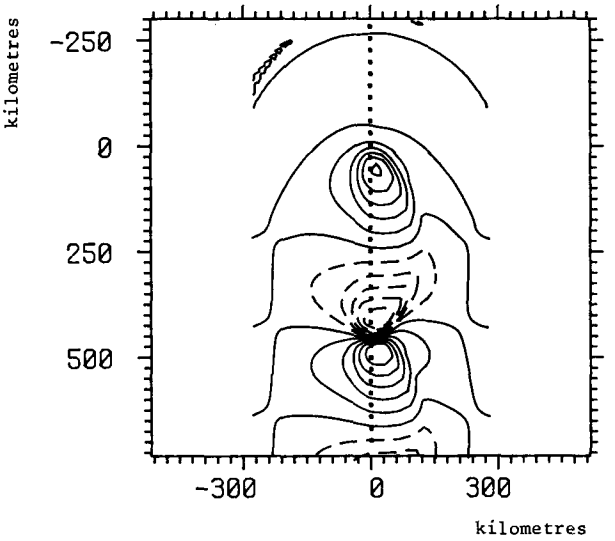

FIG. 5. The horizontal divergence field corresponding to that shown in Fig. 1, obtained by integrating the reduced equations (5.1) along the paths of 47 particles initially distributed uniformly across the storm track. The contour interval is 4.9×10^{-4} m s^{-1} and is one-sixth of the maximum response. The coordinates and scale are as in Fig. 1.

TABLE 1. A comparison between the maximum values of the horizontal divergence, given as the equivalent vertical velocity at 50 m depth, computed by the direct numerical integration method and by the Lagrangian method. In the latter model, the horizontal pressure gradient terms are dropped from the momentum equations.

Storm translation speed (m s^{-1})	Direct integration model (m s^{-1})	Lagrangian model (m s^{-1})
2.5	2.3×10^{-3} *	2.5×10^{-3}
5	3.1×10^{-3}	2.9×10^{-3}
10	1.5×10^{-3}	1.6×10^{-3}

* Laplacian smoothing in the cross-track direction was applied in this case.

wake of storm coincide with particle paths. In the wake of the storm, the particles execute inertial circles which, in the frame of reference fixed with respect to the storm, appear as cycloids—that is, circles with the translation of the storm superposed. This gives a relatively long region in which the particle is moving away from the storm and a relatively short region in which it is moving towards the storm. It is this unevenness along the track which gives rise to the uneven nature of the oscillation in the horizontal divergence field, feature 1) noted in Section 3. The parameter which controls this unevenness for a given particle is the ratio of the particle speed to the storm translation speed. When viewed collectively it is

$$A_T = \frac{\text{maximum current speed in the wake}}{\text{storm translation speed}}. \quad (5.2)$$

When A_T is small compared with 1, the oscillation along the track is even, as in the linear solution shown in Fig. 3. When $A_T = 1$, the quantity $-u_\xi$, which dominates the horizontal divergence along the center of the response, has a singularity and there is an

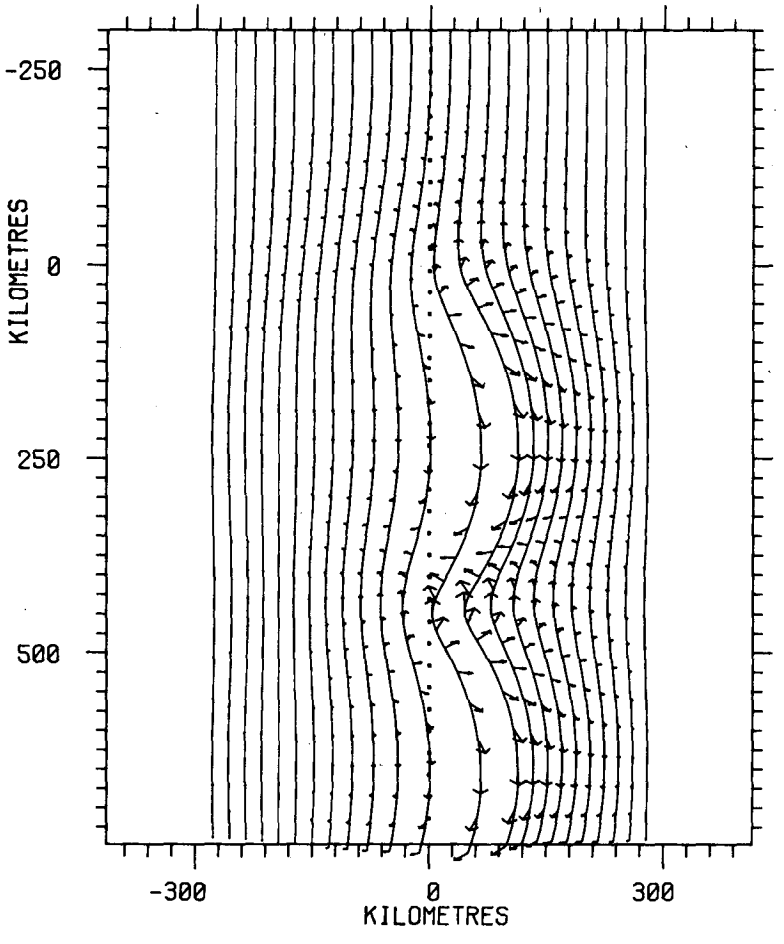

FIG. 6. Some of the computed particle paths used to obtain the horizontal divergence field shown in Fig. 5. The arrows are proportional to the particle vector velocities. The maximum particle velocity is 2.7 m s^{-1}. This compares with the storm translation speed of 5 m s^{-1}. The along-track and cross-track coordinates and their orientation are as in Fig. 1.

abrupt transition from a maximum in the downwelling to a maximum in the upwelling.

In terms of the equation (2.1), the parameter A_T measures the ratio of the $u(\partial/\partial\xi)$ term to the $U(\partial/\partial\xi)$ (i.e., $\partial/\partial t$) term in each of (2.1a) and (2.1b), indicating that it is the advection along the storm track that generates feature 1) noted in Fig. 1.

To gain some understanding of the asymmetry of the response about the storm track (feature 2 noted in Section 3), we must calculate the mean displacement of the particles from the storm track due to the action of the storm. To do this, we first integrate (5.1a) with respect to time t along a particle path, giving

$$u(t_0) - f\int_0^{t_0} v\,dt = \int_0^{t_0} X\,dt, \qquad (5.3)$$

where t_0 is some time after the passage of the storm. Letting, $\bar{y}(y_0)$ be the mean displacement perpendicular to the storm track of the particle initially at $y = y_0$ (here y is measured positively to the right of the track); then, averaging (5.3) over an inertial period in the wake of the storm gives

$$\bar{y}(y_0) \equiv \overline{\int_0^{t_0} v\,dt} = -f^{-1}\int X\,dt, \qquad (5.4)$$

where the overbar denotes the average over an inertial period in t_0, and the integral of X is taken along the particle path for the duration of the storm. In Fig. 7, $\bar{y}$ is plotted against y_0. We can calculate the depth of the upper layer h_M that is implied by these displacements by conservation of volume (mass). In fact,

$$h_M = H\left(1 + \frac{d\bar{y}}{dy_0}\right)^{-1}, \qquad (5.5)$$

where h_M is the depth of the upper layer implied by the displacements $\bar{y}$ and is the equilibrium depth of the upper layer in the wake of the storm. H is the undisturbed depth. h_M is also plotted in Fig. 7.

It is immediately clear that the maximum upward displacement of the thermocline has occurred to the right of the track. We can see from Fig. 7 that outside a distance of ~100 km from the storm track, $\bar{y}$ as a function of y_0, is approximately antisymmetric about the storm track. A particle initially on the track is, however, displaced to the left of the track (this contrasts with the prediction from linear theory that $\bar{y}$ is strictly antisymmetric about the storm track, with a particle initially on the track receiving no net displacement). Indeed, it is apparent, that the displacement of the maximum net upwelling to the right of the storm track is a consequence of the fact that the particle which receives no net displacement perpendicular to the track lies initially to the right of the track. Particles initially to the left of this pass to the left of the center of the storm and consequently the dominant contribution of X in the integral on the rhs of (5.4) is such as to give the particle a net displacement to the left of the track. To understand why this happens, we must appreciate that before rotation effects become important (that is on a time scale small compared with $1/f$), particles are accelerated to the left by the winds ahead of the storm centre.

The above argument suggests that it is the advection perpendicular to the storm track that is important in shaping the asymmetry about the storm track of the response shown in Fig. 1. We can estimate the magnitude of the $v(\partial/\partial y)$ terms using the scales discussed in Section 4. It follows that the ratio of the $v(\partial/\partial y)$ terms to the $U(\partial/\partial\xi)$ (i.e., $\partial/\partial t$) terms in (2.1) is measured by the Rossby number[2]

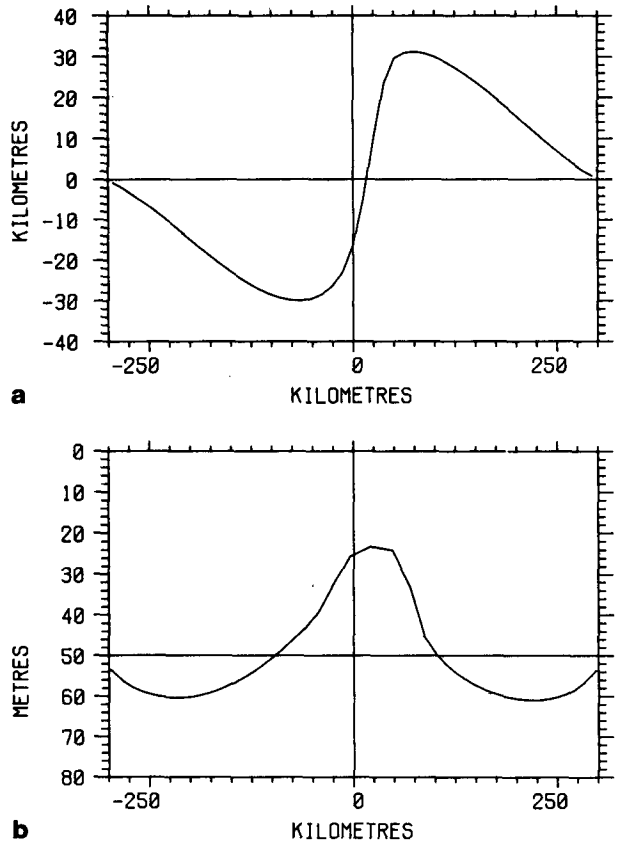

FIG. 7. (a) Mean displacement of the particles perpendicular to the storm track plotted against their initial position. The cross-track coordinate is measured in km from the storm track and positively to the right. The displacements are also measured in kilometres and positively to the right. (b) Layer depth h_M consistent by conservation of volume with the particle displacements shown in Fig. 7a. h_M is measured in m and is plotted against the cross-track coordinate which is measured in km. The cross-track coordinates of the particles have been adjusted to account for their displacements.

[2] A_T stands for along-track, P_T for perpendicular to the track. Both A_T and P_T are Rossby numbers, formed with appropriate length scales.

TABLE 2. The importance of the non-linear terms in the equations of motion. Here, U is the storm translation speed, V is the maximum current speed obtained in the appropriate model, $A_T = V/U$ measures the ratio of the along-track advection terms to the local acceleration terms, $P_T = V/Lf$ measures the ratio of the cross-track advection terms to the local acceleration terms. $L = 100$ km in each case.

	Lagrangian			Chang and Anthes (1978)		
U	V (m s^{-1})	A_T	P_T	V (m s^{-1})	A_T	P_T
5 m s^{-1}	2.7	0.54	0.36	1.7	0.34	0.23
10 m s^{-1}	2.0	0.20	0.27	1.4	0.14	0.19
2.5 m s^{-1}						
Forcing	2.1	0.84	0.28	1.2	0.48	0.16
wake	1.2	0.48	0.16	0.5	0.20	0.07

TABLE 3. Summary of results from the Lagrangian model with a comparison of the minimum layer depth predicted by the direct integration model. h_{min} is the minimum depth, $(h_M)_{min}$ is the minimum mean depth, h_M being given by (5.5). The undisturbed layer depth $H = 50$ m.

	Direct integration model	Lagrangian model			
				Maximum mean particle displacement from the track (km)	
Storm translation speed (m s^{-1})	h_{min} (m)	h_{min} (m)	$(h_M)_{min}$ (m)	Left	Right
2.5	6.8	6.8	11.9	60.2	56.4
5	12.2	13.4	23.1	30.0	31.2
10	24.0	24.2	34.5	14.7	16.0

$$P_T = V/Lf, \tag{5.6}$$

where V is the velocity scale and L is the scale of the width of the response. The time scale has been taken as $1/f$, as before.

In Table 2, velocity scales V are given for each of the three cases; that is, storms translating at 5, 10 and 2.5 m s^{-1}. In each case, these are the maximum current speeds attained in the model. In the case of the storm translating at 2.5 m s^{-1}, the forcing region and the wake are separated because of the disparity between the maximum currents in each region. The parameter $A_T = V/U$ [c.f. (5.2)] is given in each case. Of course, these values are higher than those obtained when mixing is included in the model, so estimates of the corresponding current values from Chang and Anthes (1978), who include mixing in the form of turbulent entrainment, are also given with the corresponding values for A_T. The corresponding values of P_T are also given, with $L = 100$ km, as in Section 4. It is clear that nonlinearity plays a less important role in the response to a storm translating at 10 m s^{-1} than in the other two cases, as was remarked in Section 3. This is not surprising, since the storm accelerates a given fluid particle for less time as the storm translation speed increases.

No mention has been made of the actual particle displacements $\bar{y}$ that have been calculated. These are summarized in Table 3, where details of the layer depth h as calculated in Section 3 and by the reduced Lagrangian model presented in this section, are also compared. We can see that the particle excursions are increasingly comparable to the scale of the forcing as the storm speed decreases, and vary, approximately, in inverse proportion to the storm translation speed U (linear theory predicts an exact inverse proportionality to U). It is also of interest to remark that the ratio of the oscillatory movement of the thermocline to the net displacement given by $[((h_M)_{min} - h_{min})/(H - (h_M)_{min})]$ increases as the storm speed increases, in general agreement with the findings of Geisler (1970). This ratio has values of 0.13, 0.36, 0.66 for storms translating at 2.5, 5 and 10 m s^{-1} respectively.

6. A case in which the horizontal pressure gradient terms are more important

We have seen that the horizontal pressure gradient terms do not play a significant role in shaping the structure and amplitude of the response shown in Fig. 1. In this section, we make comparisons with a case in which these terms are more important. The model derived in Section 3 was run with $c = 2$ m s^{-1} and $H = 100$ m (corresponding to a temperature difference between the two layers of 20°C) all other factors, including the wind stress forcing (2.3), remaining the same. In this case the wave speed c is double that previously used so that on the basis of the scale anal-

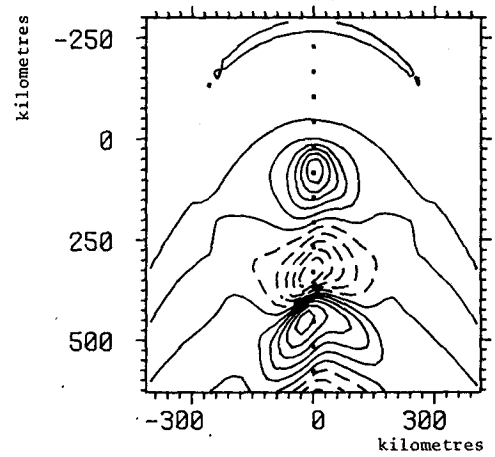

FIG. 8. The horizontal divergence field expressed as the equivalent vertical velocity at the undisturbed layer depth H. In this case $H = 100$ m and the reduced gravity g' is such that the wave speed $(g'H)^{1/2}$ is 2 m s^{-1}. The storm translation speed is 5 m s^{-1}. The contour interval is 4.1×10^{-4} m s^{-1} and is one-sixth of the maximum response. The coordinates and scale are as in Fig. 1.

ysis given in Section 4, we would expect the horizontal pressure gradient terms to be four times more important in the equations of motion. Fig. 8 shows the computed horizontal divergence field for a storm translating at 5 m s^{-1} and is directly comparable with Fig. 1, discussed in Section 3. Two important differences emerge:

1) The dominant wavelength of the oscillation along the track has been reduced from near 420 km to near 370 km.

2) There is only a slight bias to the right of the track under the storm (more obvious from the contours of h shown in Fig. 9) with a marked bias to the left of the track developing in the wake of the storm.

Despite these differences, the basic uneven nature of the oscillation along the storm track (feature 1) noted in Section 3) is still apparent.

The first difference, that in the wavelength along the track, is easy to understand. We saw in Section 4, when discussing the response to a storm translating at 2.5 m s^{-1}, how the wavelength along the track was reduced from the inertial wavelength $2\pi U/f$ by a factor $(U^2 - c^2)^{1/2}/U$. This factor has the value 0.92 when $U = 5$ m s^{-1} and $c = 2$ m s^{-1}, which predicts an along-track wavelength of 386 km. This reduction is attributable to the along-track pressure gradient term p_ξ. The further reduction to 370 km can be attributed to the cross-track pressure gradient term p_y.

We can estimate the ratio of the pressure gradient to the Coriolis terms by $(g'\nabla h)/fV$, where V is the maximum current speed found in the model (1.2 m s^{-1} in this case) and for ∇h we take the maximum gradient of h along the line A–B shown in Fig. 9. This line extends perpendicularly across the storm track 200 km behind the storm center. This ratio has value of ~0.16 in this case. This compares with the corresponding ratio of 0.05 estimated for the calculations described in Section 3 with $c = 1$ m s^{-1} and $U = 5$ m s^{-1}. As we would expect, this ratio is approximately quadrupled when the wave speed c is doubled, while all other factors remain the same, in agreement with our expectations on the basis of the scale analysis given in Section 4 [c.f. (4.3)].

The second difference, regarding the asymmetry of the response in the wake about the storm track, is less easy to understand and will not be discussed here.

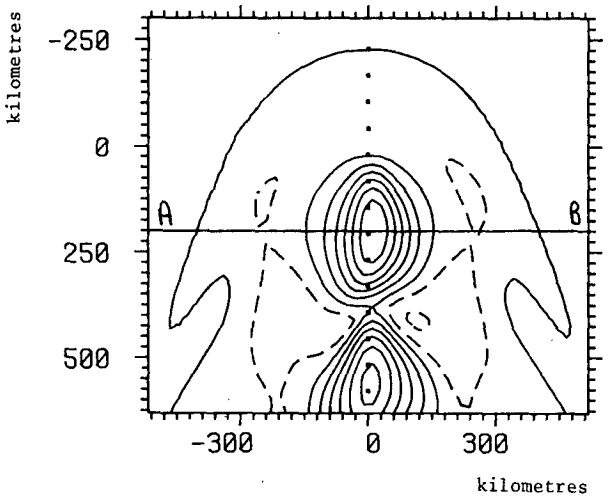

FIG. 9. The layer depth h corresponding to the horizontal divergence field shown in Fig. 8. The contour interval is 7 m and is one-sixth of the maximum displacement from the undisturbed layer depth of 100 m. The dashed contours denote deepening of the layer. The zero contour and contours denoting shallowing of the layer are shown as solid lines. The coordinates and scale are as in Fig. 1. The line A-B is referred to in the text.

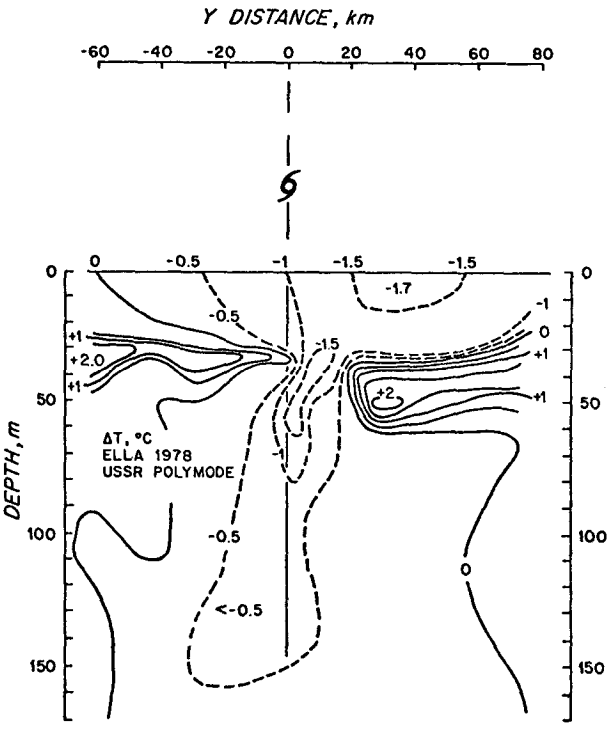

FIG. 10. The response of subsurface temperature across the track of hurricane Ella (1978) after Fedorov *et al.* (1979). The contour interval is 0.5°C, negative values are dashed. *XBT* casts were made at approximately 20 km intervals along a section approximately one day before and after the passage of the hurricane. Note the displacement to the right of the track (denoted by the hurricane symbol) of the upwelling column (taken from Price, 1981).

7. Forcing with an asymmetric storm

To investigate the effect of forcing with an asymmetric storm, the model described in Section 3 was run with the surface wind stress (2.3) multiplied by the factor $(1 + 0.3\cos\theta)$, where θ is measured from a semi-axis extending from the storm center, perpendicular to the storm track and outwards to the right,

when viewing the storm from behind. It is usual for hurricanes to have this sort of asymmetry, with the strongest winds being found to the right of the track, although the factor 0.3 represents a case of strong asymmetry. Two cases were considered, that of 1) $c = 1$ m s^{-1}, $U = 5$ m s^{-1} and 2) $c = 2$ m s^{-1}, $U = 5$ m s^{-1}. Although the computed horizontal divergence field (not shown here) is a little more biased to the right of the storm track than in the corresponding cases with symmetric forcing discussed in Sections 3 and 6, respectively, the basic response is changed little from that discussed before. This suggests that in these cases, asymmetry in the storm forcing is not important, in comparison with the nonlinear dynamics, in determining the asymmetry of the response.

8. Summary and discussion

We have seen that the nonlinear terms in the equations of motion (2.1) introduce two important features to the character of the oscillation in the wake of the storm:

1) There is a rapid transition from a maximum in the downwelling phase to a maximum in the upwelling phase, followed by a gradual transition to the next downwelling maximum.

2) The maximum of the response is displaced to the right of the storm track, although when the horizontal pressure gradient terms in (2.1a) and (2.1b) play a more important role in the equations, the maximum response in the wake, behind the storm, shifts to the left of the track.

A Lagrangian integration technique, following individual fluid particles, has been used to show that feature 1) is attributable to advection of momentum along the track and that feature 2) is associated with the cross-track advection terms. It has also been shown that the nonlinear dynamics can be more important than an asymmetry in the storm forcing in producing an asymmetric response.

Finally in this paper, we ask whether or not any of the above mentioned features are found in observations of the ocean's response to particular hurricanes. Within the limited set of observational studies available, (Price, 1981 contains a general review of such studies) there are some examples in which the upwelling column is displaced to the right of the storm track (there are no examples of a clear-cut displacement to the left of the track). A particularly fine example is provided by the study undertaken and documented by Schramm (1979) of the response to

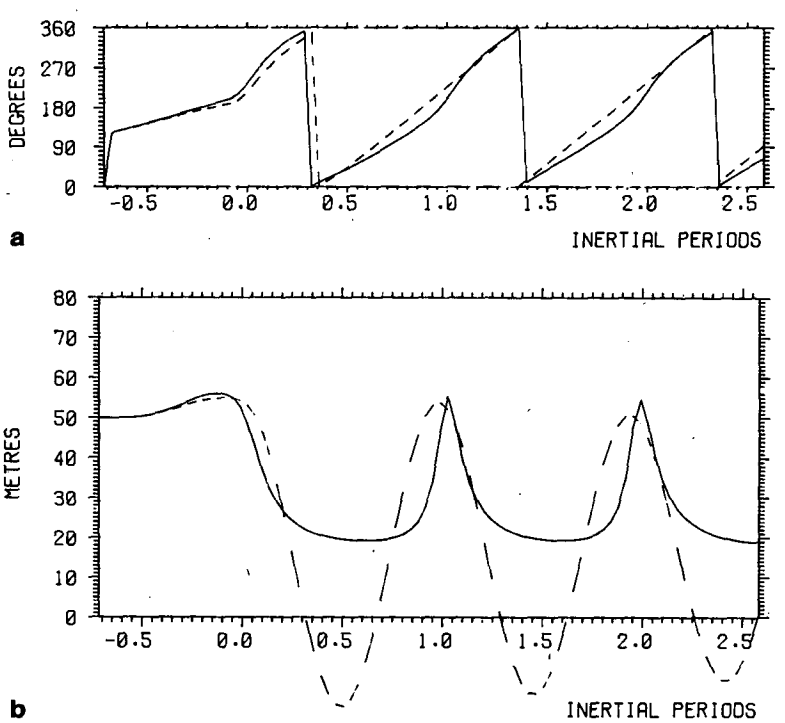

FIG. 11. (a) Current direction along the storm track obtained from the same numerical experiment as Fig. 1. Direction is measured clockwise from the direction of motion of the storm with the current flowing from the direction indicated. The dashed line shows the result obtained by integrating the linearized equations, all other factors remain the same. The origin of the time axis is at the center of the storm; (b) As in a, except that here the layer depth h is shown. This can be thought of in terms of temperature below the wind-mixed layer.

typhoon Phyllis of 1975. In this case, the upwelling column is centered ~40 km to the right of the track with half-width ~ 100 km, in broad agreement with the model results presented here (cf. Fig. 1). Fig. 10 is taken from Price (1981) and shows the difference in temperature along a section across the path of hurricane Ella of 1978, between XBT casts made approximately one day before and one day after the passage of the storm (Fedorov *et al.*, 1979). A rightward bias in the upwelling column is again apparent.

Observations of feature 1) noted above requires a good time series of data in a region sufficiently close to the storm track that the surface current reaches a value that is a significant fraction of the storm translation speed, i.e., we need the parameter A_T [cf. (5.2)] to be significantly different from zero. The only likely candidate available at the present time would seem to be the data set recorded by the EB-10 buoy during the passage of hurricane Eloise in 1975 (see Johnson and Withee, 1978 for a presentation of this data set). In this case, the storm translation speed at the time of crossing the buoy was near 8.5 m s^{-1}. Unfortunately, current speed was only measured by one sensor, nominally at a depth of ~50 m. It recorded a maximum value of 0.8 m s^{-1} at which time the temperature measured by the sensor was within ~0.3°C of that measured by a sensor at a nominal depth of 2 m. This suggests that 0.8 m s^{-1} may be a representative value of the current speed within the mixed layer. This gives a value for $A_T = 0.8/8.5$ of only ~0.1 so that nonlinear effects are likely to be small and easily obscured by other factors.

Fig. 11 shows time series along the storm track obtained from the numerical model described in Section 3. In this case, $A_T = 0.54$ (this based on a maximum computed current speed of 2.7 m s^{-1}, the storm translation speed being 5 m s^{-1}). The equivalent plots obtained by integrating the linearized equations are also given, highlighting the nonlinear effects [these are associated with feature 1) noted above]. It is hoped that these figures will provide a guide to interpreting observations in a more highly nonlinear case than that recorded by the EB-10 buoy.

Acknowledgments. I am grateful to the Science and Engineering Research Council of the U.K., and to the U.K. Meteorological Office for financial support. I should also like to thank Dr. A. E. Gill for his constant encouragement and advice and Dr. J, F. Price for his comments on an early version of the manuscript. I am also most grateful to the National Oceanic and Atmospheric Administration, Washington DC, for providing me with the data from the EB-10 buoy.

APPENDIX

We describe here the method used to calculate the divergence and relative vorticity from the velocity field obtained as output from the Lagrangian model described in Section 5.

Consider a scalar field $F[x(s, t), y(s, t)]$. Here $[x(s, t), y(s, t)]$ is the position at time t of the particle initially at position (x_0, s), the line x_0 = constant being the initial line of particles ahead of the storm. We know F as a function of s and t, and we wish to know its derivatives with respect to x and y. We can then take $F \equiv u$ and $F \equiv v$ and combine the calculated derivatives with respect to x and y, appropriately, to form the divergence $u_x + v_y$ and the relative vorticity $v_x - u_y$.

Using the chain rule,

$$(\partial_s F, \partial_t F) = (\partial_x F, \partial_y F)\begin{pmatrix} \partial_s x & \partial_t x \\ \partial_s y & \partial_t y \end{pmatrix}, \qquad \text{(A1)}$$

where $\partial_s \equiv \partial/\partial_s$ etc.

Inverting (A1) we have

$$(\partial_x F, \partial_y F) = \frac{1}{D}(\partial_s F, \partial_t F)\begin{pmatrix} \partial_t y & -\partial_t x \\ -\partial_s y & \partial_s x \end{pmatrix}. \qquad \text{(A2)}$$

where

$$D = \frac{\partial x}{\partial s}\frac{\partial y}{\partial t} - \frac{\partial x}{\partial t}\frac{\partial y}{\partial s}.$$

In applying (A2) numerically to the data output from the model, we can parameterize the coordinates in such a way that the distance between neighboring points at fixed s is 1, and similarly at fixed t. This useful observation simplifies the computations. In particular, by using centred differencing to estimate the derivatives in (A2) we can now achieve a second-order approximation.

REFERENCES

Arakawa, A., and V. R. Lamb, 1977: Computational design of the UCLA General Circulation Model. *Methods in Computational Physics*, Vol. 17, J. Chang, Ed., Academic Press.

Chang, S. W., and R. A. Anthes, 1978: Numerical simulations of the ocean's nonlinear, baroclinic response to translating hurricanes. *J. Phys. Oceanogr.*, **8**, 468–480.

Fedorov, K. N., A. A. Varfolomeev, A. I. Ginzburg, A. G. Zatsepin, A. Yu. Krashopevtsev, A. G. Ostrovsky and V. E. Skylarov, 1979: Thermal reaction of the ocean on the passage of hurricane Ella. *Okeanologiya*, **19**, 992–1001.

Geisler, J. E., 1970: Linear theory of the response of a two-layer ocean to a moving hurricane. *Geophys. Fluid Dyn.*, **1**, 249–272.

Greatbatch, R. J., 1982a: On the response of the ocean to a moving storm: Parameters and scales. Submitted to *J. Phys. Oceanogr.*

——, 1982b: On the response of the ocean to a moving storm: Turbulent mixing effects. (In preparation).

Johnson, A., and J. W. Withee, 1978: Ocean data buoy measurements of hurricane Eloise. *Mar. Tech. Soc. J.*, **12**, 14–20.

Price, J. F., 1981: On the upper ocean response to a moving hurricane. *J. Phys. Oceanogr.*, **11**, 153–175.

Schramm, W. G., 1979: Airborne expendable bathythermograph observations immediately before and after the passage of typhoon Phyllis in August of 1975. Dept. of Navy, NAVENVPREDRESFAC (Draft).